Thin Solid Films 520 (2011) 1656–1659

Contents lists available at ScienceDirect

Thin Solid Films

journal homepage: www.elsevier.com/locate/tsf

Resistive switching characteristics of ytterbium oxide thin film for nonvolatile memory application

Hsueh-Chih Tseng [a], Ting-Chang Chang [a,b,*], Jheng-Jie Huang [a], Yu-Ting Chen [c], Po-Chun Yang [c], Hui-Chun Huang [d], Der-Shin Gan [d], New-Jin Ho [d], Simon M. Sze [e], Ming-Jinn Tsai [f]

[a] Department of Physics, National Sun Yat-Sen University, Kaohsiung, 804, Taiwan, ROC
[b] Center for Nanoscience & Nanotechnology, National Sun Yat-Sen University, Kaohsiung, 804, Taiwan, ROC
[c] Department of Electro-Optical Engineering, National Sun Yat-Sen University, Kaohsiung, 804, Taiwan, ROC
[d] Department of Materials Science and Engineering, National Sun Yat-Sen University, Kaohsiung, 804, Taiwan, ROC
[e] Institute of Electronics, National Chiao Tung University, Hsin-Chu, 300, Taiwan, ROC
[f] Electronics and Opto-electronics Research Laboratories, Industrial Technology Research Institute, Hsinchu, Taiwan, ROC

ARTICLE INFO

Available online 23 July 2011

Keywords:
Nonvolatile resistance switching memory
RRAM
Yb_2O_3
Forming

ABSTRACT

This paper studies the effects of both the positive and negative forming processes on the resistive switching characteristics of a Pt/Yb_2O_3/TiN RRAM device. The polarity of the forming process can determine the transition mechanism, either bipolar or unipolar. Bipolar behavior exists after the positive forming process, while unipolar behavior exists after the negative forming process. Furthermore, the bipolar switching characteristics of the Pt/Yb_2O_3/TiN device can be affected by using a reverse polarity forming treatment, which not only reduces the set and reset voltage, but also improves the on/off ratio.

Crown Copyright © 2011 Published by Elsevier B.V. All rights reserved.

1. Introduction

Resistive random access memory (RRAM) has attracted considerable interest for the next generation of nonvolatile memory devices due to its simple structure, low operation voltage and process compatibility with the present CMOS industry [1]. Many materials have been demonstrated to achieve resistive switching characteristics, such as perovskite oxides $Pr_{0.7}Ca_{0.3}MnO_3$ and $SrZrO_3$ [2,3] and binary metal oxides such as Al_2O_3, ZrO_2, MnO_2, CuO, NiO and TiO_2 [4–9]. Two dominant resistance switching mechanisms have been proposed. One is oxygen vacancy nucleation at a metal/oxide interface [10,11]. The other mechanism is the conductive filament model, which describes the formation/rupture of a metallic filament using a metal such as Cu or Ag acting as mobile ions in the oxide [12]. Recently, rare earth (RE) metal oxides, which are used as a high-k gate insulator for advanced complementary metal-oxide-semiconductor (CMOS) technology [13,14], have been demonstrated to exhibit resistance switching phenomena [15,16]. One of the RE metal oxides, ytterbium oxide (Yb2O3), is attractive as a gate dielectric in CMOS devices because of its dielectric constant of 15, larger energy band gap (>5 eV), and predicted chemical and thermal stability with Si. Therefore, it also has been explored for semiconductor applications including memory devices, logical devices and optoelectronic devices [17]. Up to now, the application of Yb2O3 in the resistive switching field has not been researched.

* Corresponding author at: Department of Physics, National Sun Yat-Sen University, 70 Lien-Hai Road, Kaosiung, Taiwan 80424, ROC. Tel.: +886 7 5252000 3708; fax: +886 7 5253709.
E-mail address: tcchang@mail.phys.nsysu.edu.tw (T.-C. Chang).

This work investigates resistance switching characteristics in a Pt//Yb_2O_3/TiN structure by using both the positive forming (PF) and negative forming (NF) processes. In addition, after the PF process, a reverse polarity forming (RPF) treatment is also studied. A mechanism is proposed to explain the influence on resistive switching characteristics of the Yb_2O_3-based RRAM of the device after a PF process both with and without an additional RPF treatment.

2. Experiment

Yb_2O_3 thin film of 20 nm thickness was deposited on a TiN/Si substrate by reactive magnetron RF sputtering an Yb_2O_3 target in Ar (30 sccm) ambient at room temperature. The RF sputtering power and pressure of the sputter system were set to 150 W and 4 mTorr. Next, the Pt top electrode (TE) was deposited and patterned by the liftoff process. High-resolution transmission electron microscopy (HRTEM) was used to observe lattice images of the Yb_2O_3 thin film, and X-ray photoelectron spectroscopy (XPS) was employed to determine the chemical bonding state of the Yb_2O_3 thin films. The standard sample was PF treated, whereas the control sample used as reference was a standard sample with additional RPF treatment, and will be referred to as standard and control samples hereafter. Additionally, another sample activated by the NF process was used to clarify the effects of the RPF treatment. The temperature dependence of resistance in the low resistance state (LRS) of these three samples was observed. All electrical characteristics were measured over an 8 μm × 8 μm cell size with an Agilent B1500 semiconductor parameter analyzer. During

0040-6090/$ – see front matter. Crown Copyright © 2011 Published by Elsevier B.V. All rights reserved.
doi:10.1016/j.tsf.2011.07.026

these measurements, bias was applied to the TiN bottom electrode (BE) while the Pt top electrode (TE) was grounded.

3. Results and discussion

In order to ascertain the switching mechanism, HRTEM was performed to analyze this structure. Many studies have indicated that the grain boundary can induce multiple conductive paths. As shown in Fig. 1(a), many grain boundaries are observed in the as-deposited Yb_2O_3 thin film. Therefore, multiple conductive paths can be formed, such as Yb or semiconducting YbO_x. Fig. 1(b) shows the XPS analysis which investigates the chemical states of ytterbium and oxygen. The Yb $4d_{5/2}$ spectrum indicates a coexistence of Yb^{+3} and metallic Yb in Yb_2O_3, with Yb^{+3} (Yb^{+3} at 184.1 eV) making up the majority and metallic Yb (Yb^{0+} at 182 eV) the minority. Furthermore, the O1s spectrum indicates a similar coexistence of lattice oxygen ions, with a majority of O^{-2} (O^{-2} at 529.1 eV) and a smaller amount of nonlattice oxygen ions (O^{0+} at 531 V). Kang et al. [18] ascribes the forming free behavior in ZnO-based devices to the abundant oxygen vacancies and the pre-existing nonlattice oxygen ions in the ZnO films. These results imply that the forming process is mandatory for this device before use as a memory device.

As mentioned above, the forming process is necessary to activate the RRAM device. During the PF process, as shown in the inset of Fig. 2, a positive DC bias of about 14 V was applied to the BE with a current compliance of 1 μA. Then, many conductive paths occurred as a result of dielectric breakdown, with the resistance state (RS) then transforming from initial high resistance state ($HRS_{initial}$) to initial LRS ($LRS_{initial}$). This can be attributed to a dynamic process of breaking the chemical bonds to generate oxygen vacancies and nonlattice oxygen ions. Hence, the nonlattice oxygen ions can drift towards the anode and form TiO_x at the TiN/oxide interface due to the electrical field [19,20], resulting in many defects or oxygen vacancies along the leakage paths [21], as shown in the inset schematic diagram of Fig. 2. In addition, Fig. 2 shows the temperature dependence of resistance after activating the device, where the $LRS_{initial}$ decreases when the ambient temperature increases, as is typical of semiconductor behavior [22]. Because of the interface formation, the voltage across the device can be divided between the bulk and interface region, which prevents the bulk region from continually generating more oxygen ions. From this result, it can be inferred that the conductive paths consist of semiconducting oxide or oxygen vacancies.

Fig. 3 shows the typical bipolar switching behavior of the Pt/Yb_2O_3/TiN device. The transition between LRS and HRS is observed for 100 cycles by using dc voltage sweeping mode. First, during the set process, a predetermined sweeping voltage of about 2 V with 10 mA current compliance was applied, after which there is a sudden increase in current observed at about 1.5 V, which is defined as V_{set}. In a subsequent sweep, the LRS was achieved during backward sweeping from 2 V to 0 V. In a similar fashion during the reset process, the RS can be restored to HRS by using a negative sweeping voltage of about −2 V, with the current starting to decrease at about −1.4 V, which is defined as V_{reset}. In a subsequent sweep, the HRS was achieved during the backward sweeping from −2 V to 0 V. Recent studies have indicated that the bipolar resistance switching is related to the redox reaction near the anode-electrode/oxide interface [19], as shown in the inset of Fig. 3.

However, during RPF treatment, as shown in the inset of Fig. 4, a higher and reverse polarity dc bias with a 10 mA current compliance was applied to the standard device. The anode-electrode interface layer decomposed and the adjacent conductive path(s) rupture and reform, as shown in the inset schematic diagram of Fig. 4. First, when the bias increases to about −3 V, there is a noticeable transformation in RS, which suddenly transforms from LRS to the new $HRS_{initial}$. This violent RS transformation of RPF reveals that the multiple and redundant conducting paths are eliminated by the Joule Heating effect [23]. Some research has indicated that the reset behavior is due to the annihilation of oxygen vacancies or oxidation of the conductive paths [20,21,24]. Subsequently, when the bias continues to increase, at about −5 V the RS transforms again from the new $HRS_{initial}$ to new $LRS_{initial}$, which is similar to the forming process. Then, the oxygen

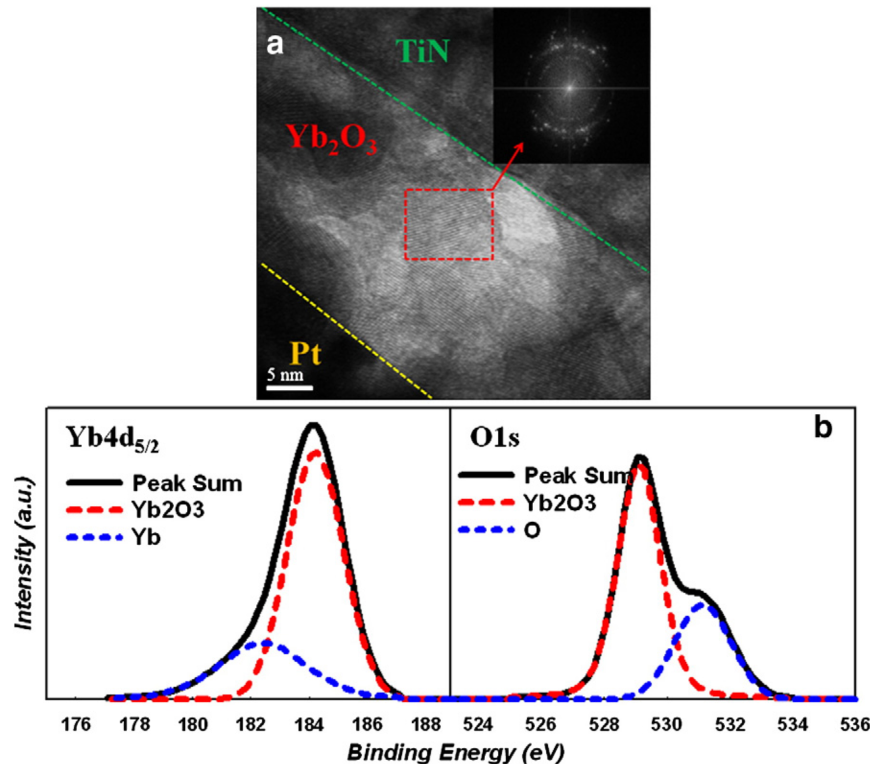

Fig. 1. (a) High-resolution transmission electron microscopy (HRTEM) image. (b) XPS spectra of Yb 4 d5/2 and O 1 s.

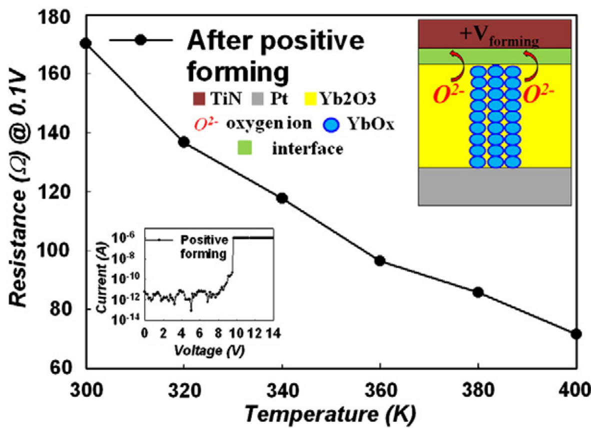

Fig. 2. Temperature dependence resistance in $LRS_{initial}$ for the standard sample, with a 0.1 V reading voltage. The inset shows the positive forming I–V curve and schematic diagram of the measurement system.

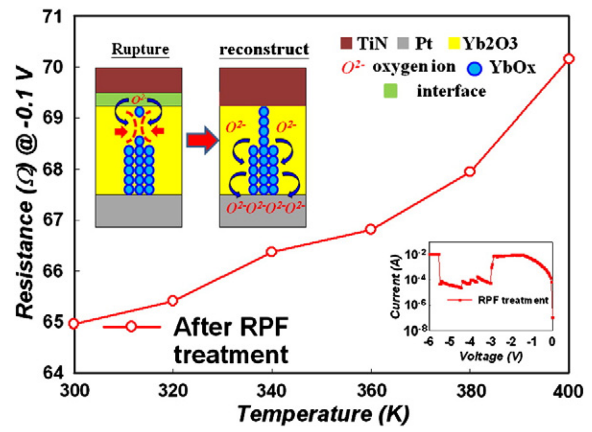

Fig. 4. Temperature dependence resistance in $LRS_{initial}$ for the control sample, with a −0.1 V reading voltage. The inset shows the RPF treatment I–V curve and the schematic diagram of the measurement system.

vacancies and oxygen ions can be generated again; moreover, these oxygen ions drift to Pt and can be chemisorbed at the grain boundary or penetrate through the Pt layer [21,24]. Fig. 4 shows that the temperature dependence of resistance in the new $LRS_{initial}$ increases when the ambient temperature increases. The interface of TiN has decomposed; indeed, Pt cannot be thoroughly oxidized. The cross voltage can act completely on the bulk region, so there is a metallic behavior of the conductive paths [22]. Furthermore, a few cycles of unipolar switching phenomena appear momentarily after the RPF treatment.

The transition between the LRS and HRS of the control sample was observed for 100 cycles by using the same dc voltage sweeping mode as the standard sample, as shown in Fig. 5. Compared with the standard samples, the V_{set} and V_{reset} of the control samples are lower. The inset of Fig. 5 shows that, after the bipolar switching mode, the temperature dependence of resistance, including LRS and HRS, decreases when ambient temperature increases, again typical of semiconducting behavior [22]. The oxygen ions drift towards TiN and reconstruct the interface layer during the set process. Thus, a different transition of RS induces change from metallic behavior to semiconducting behavior because the TiN interface is still the redox reaction region. The force required to break the chemical bonds of the set process is weaker than the forming process, resulting in a thinner interface layer.

The negative differential (NDF) region of on current, which is located in the negative bias region, affects the growth rate of HRS. Fig. 5 indicates that the lower V_{reset} induces the longer NDF region, and the larger HRS of the control sample can be achieved by applying the same stopping voltage, as shown in Fig. 6. In addition, because many studies have indicated that reconstruction of the conductive path(s) occurs in only a single path [25], this larger HRS can be attributed to a decrease of conductive paths. Thus, the redox reaction is more concentrated at residual conductive paths, as shown in the inset of Fig. 6. Generally speaking, the set process is a soft breakdown phenomenon, and is related to metal/oxide interfacial quality and thickness. For this reason, the thinner interface layer can not only cause a reduced V_{set}, but can also cause lower LRS.

The RPF treatment in Yb_2O_3 thin film causes the decomposition of the anode-electrode interface layer and the rupture/reformation of the conductive path(s). For comparison with the RPF treatment device, the negative forming (NF) process device is shown in the inset of Fig. 7. The RS changes from $HRS_{initial}$ to $LRS_{initial}$ by applying a negative voltage of about −14 V to the BE. According to this polarity, the oxygen ions migrate towards TE. Many studies have indicated that the oxidation of Pt is difficult to achieve [20,21,24]. Hence, as shown in the inset schematic diagram of Fig. 2, the conductive paths may consist of Yb metal atoms, such as the NiO-based system [25,26]. Additionally, Fig. 7 shows that this $LRS_{initial}$ increases as ambient temperature rises, which is similar to typical metallic behavior. A comparison of the temperature dependence of $LRS_{initial}$ for PF and NF shows opposite tendencies.

Finally, after the NF process, the RS switching behaviors have a clear transformation from a bipolar to a unipolar mechanism. Fig. 8 shows the typical unipolar switching behaviors of the $Pt/Yb_2O_3/TiN$

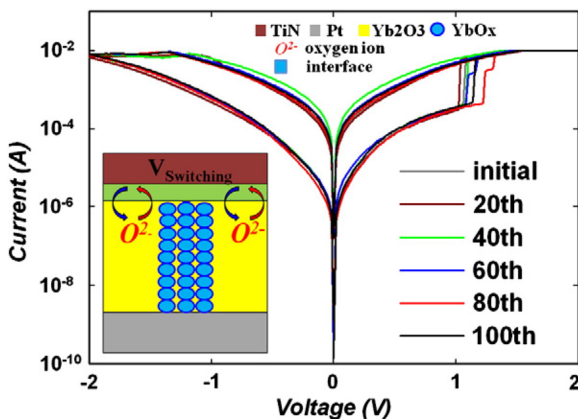

Fig. 3. Typical bipolar resistive switching I–V curves for the standard sample. The inset shows a schematic diagram of the switching mechanism.

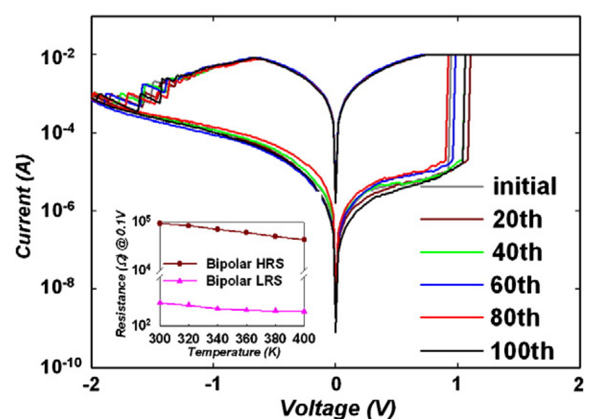

Fig. 5. Typical bipolar resistive switching I–V curves for the control sample. The inset shows temperature dependence resistance in LRS and HRS.

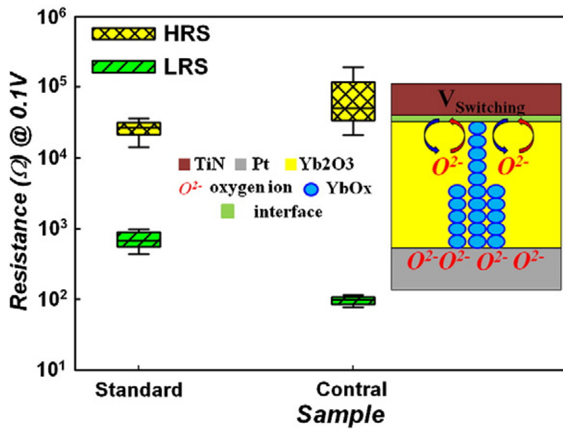

Fig. 6. LRS and HRS statistics for standard and control samples for 100 cycles in dc sweeping mode, with a 0.1 V reading voltage. The inset shows a schematic diagram of the switching mechanism.

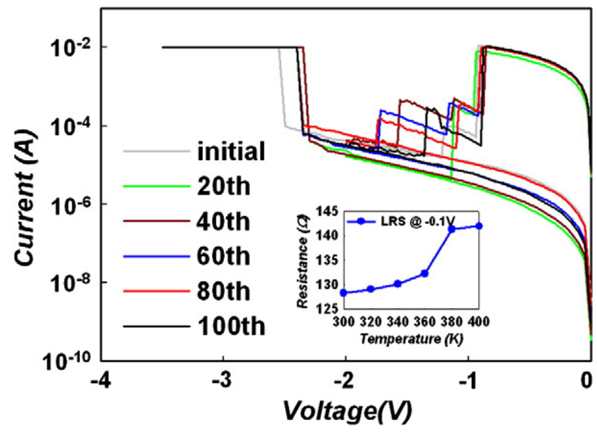

Fig. 8. Typical unipolar resistive switching I–V curves for the sample activated by negative forming process. The inset shows temperature dependence resistance in LRS, with a −0.1 V reading voltage.

device. The transition between LRS and HRS was observed for 100 cycles by using dc voltage sweeping mode. First, starting at 0 V and sweeping to −3.5 V with a 10 mA current compliance, a sudden increase of leakage current is observed at a voltage of about −2.3 V, defined as the $V_{uni\text{-}set}$, with the RS able to be stored in LRS. Then, starting again at 0 V and sweeping to −2 V a sudden drop of current around −1 V was observed, defined as $V_{uni\text{-}reset}$, with a restoration of the RS to the HRS. Therefore, as shown in the inset of Fig. 8, the temperature dependence of LRS indicates that the resistance increases as ambient temperature rises. This temperature dependence phenomenon in the conductive path is similar to RPF treatment, which is typically metallic in behavior.

4. Conclusion

In conclusion, the effect of a PF and a NF on resistive switching characteristics of a $Pt/Yb_2O_3/TiN$ RRAM device has been investigated. Results indicate that the switching mechanism is dependent on the polarity of the forming process, and also affects the metal/oxide interface layer decomposition and formation. Therefore, applying the reverse polarity forming treatment for the standard sample which has been activated by the PF process can obtain better bipolar switching characteristics such as lower set and reset voltages, and a larger on/off ratio. This work demonstrates the improvement of switching characteristics by using the reverse polarity forming treatment.

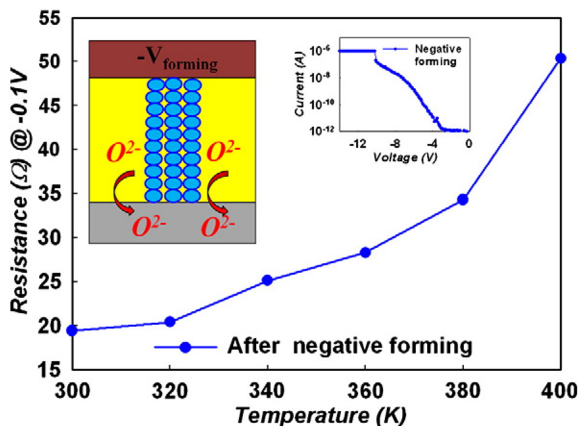

Fig. 7. Temperature dependence resistance in $LRS_{initial}$ for the sample activated by negative forming process, with a −0.1 V reading voltage. The inset shows the negative forming I–V curve and the schematic diagram of the measurement system.

Acknowledgment

This work was performed at National Science Council Core Facilities Laboratory for Nano-Science and Nano-Technology in Kaohsiung-Pingtung area and was supported by the National Science Council of the Republic of China under contract nos. NSC-99-2120-M-110-001 and NSC-97-2112-M-110-009-MY3.

References

[1] K. Szot, W. Speier, G. Bihlmayer, R. Waser, Nat. Mater. 5 (4) (2006) 312.
[2] A. Sawa, T. Fujii, M. Kawasaki, Y. Tokura, Appl. Phys. Lett. 85 (2004) 4073.
[3] C.Y. Liu, P.H. Wu, A. Wang, W.Y. Jang, J.C. Young, K.Y. Chiu, T.Y. Tseng, IEEE Electron Device Lett. 26 (6) (2005) 351.
[4] C.Y. Lin, C.Y. Wu, C.Y. Wu, C. Hu, T.Y. Tseng, J. Electrochem. Soc. 154 (9) (2007) G189.
[5] C.Y. Lin, C.Y. Wu, C.Y. Wu, T.C. Lee, F.L. Yang, C. Hu, T.Y. Tseng, IEEE Electron Device Lett. 28 (5) (2007) 366.
[6] M.K.Y.J.W. Park, T.K. Ko, L.K. Lee, Appl. Phys. Lett. 95 (2009) 042105.
[7] R. Dong, D.S. Lee, W.F. Xiang, S.J. Oh, D.J. Seong, S.H. Heo, H.J. Choi, M.J. Kwon, S.N. Seo, M.B. Pyun, M. Hasan, H. Hwang, Appl. Phys. Lett. 90 (2007) 42107.
[8] G.S. Park, X.S. Li, D.C. Kim, R.J. Jung, M.J. Lee, S. Seo, Appl. Phys. Lett. 92 (2007) 222103.
[9] B.J. Choi, D.S. Jeong, S.K. Kim, C. Rohde, S. Choi, J.H. Oh, H.J. Kim, C.S. Hwang, K. Szot, R. Waser, B. Reichenberg, S. Tiedke, J. of Phys. Lett. 98 (2005) 33715.
[10] J.J. Yang, F. Miao, M.D. Pickett, D.A.A. Ohlberg, D.R. Stewart, C.N. Lau, R.S. Williams, Nanotechnology 20 (2009) 215201.
[11] C. Yoshida, K. Kinoshita, T. Yamasaki, Y. Sugiyama, Appl. Phys. Lett. 93 (2008) 042106.
[12] C. Schindler, G. Staikov, R. Waser, Appl. Phys. Lett. 94 (2009) 072109.
[13] A. Fissel, M. Czernohorsky, H.J. Osten, Superlattices Microstruct. 40 (2006) 551.
[14] L. Marsella, V. Fiorentini, Phys. Rev. B 69 (2004) 172103.
[15] X. Cao, X. Li, X. Gao, W. Yu, X. Liu, Y. Zhang, L. Chen, X. Cheng, J. Phys. Lett. 106 (2009) 073723.
[16] K.C. Liu, W.H. Tzeng, K.M. Chang, Y.C. Chan, C.C. Kuo, C.W. Cheng, Microelectron. Reliab. 50 (2010) 670.
[17] T.M. Pan, W.S. Huang, Appl. Surf. Sci. 255 (2009) 4979.
[18] N. Xu, L. Liu, X. Sun, X. Liu, D. Han, Y. Wang, R. Han, J. Kang, B. Yu, Appl. Phys. Lett. 92 (2008) 232112.
[19] S.Y. Wang, D.Y. Lee, T.Y. Tseng, C.Y. Lin, Appl. Phys. Lett. 95 (2009) 112904.
[20] S. Yu, H.-S. Philip Wong, IEEE Electron Device Lett. 31 (12) (2010) 1455.
[21] L. Goux, P. Czarnecki, Y.Y. Chen, L. Pantisano, X.P. Wang, R. Degraeve, B. Govoreanu, M. Jurczak, D.J. Wouters, L. Altimime, Appl. Phys. Lett. 97 (2010) 243509.
[22] C. Chen, Y.C. Yang, F. Zeng, F. Pan, Appl. Phys. Lett. 97 (2010) 083502.
[23] S.H. Chang, J.S. Lee, S.C. Chae, S.B. Lee, C. Liu, B. Kahng, D.-W. Kim, T.W. Noh, Phys. Rev. Lett. 102 (2009) 026801.
[24] L. Goux, z.X.P. Wang, Y.Y. Chen, L. Pantisano, N. Jossart, B. Govoreanu, J.A. Kittl*, M. Jurczak, L. Altimime, D.J. Wouters, Electrochem. Solid-State Lett. 14 (6) (2011) H244.
[25] U. Russo, D. Ielmini, C. Cagli, A.L. Lacaita, IEEE Trans. Electron Devices 56 (2) (2009) 193.
[26] H. Shima, F. Takano, H. Akinaga, Tamai Yukio, I.H. Inoue, H. Takagi, Appl. Phys. Lett. 91 (2007) 012901.